Repeatability and reproducibility of prospective motion- and shim corrected 2D glycoCEST MRI

Gizeaddis Lamesgin Simegn[1,2], Ali Alhamud[2,3,4], Andre J. W. van der Kouwe[2,5,6], Ernesta Meintjes[2,3,7,8], Frances Robertson[2,3,7]

[1]School of Biomedical Engineering, Jimma Institute of Technology, Jimma University, Jimma, Ethiopia; [2]UCT Medical Imaging Research Unit, Division of Biomedical Engineering, Department of Human Biology, University of Cape Town, Cape Town, South Africa; [3]Cape Universities Body Imaging Centre (CUBIC), Cape Town, South Africa; [4]Al-Zintan University, Faculty of Medicine, Alzintan, Libya; [5]Athinoula A. Martinos Center for Biomedical Imaging/MGH, Charlestown, MA, USA; [6]Department of Radiology, Harvard Medical School, Boston, MA, USA; [7]Biomedical Engineering Research Centre, [8]Neuroscience Institute, University of Cape Town, Cape Town, South Africa

Correspondence to: Frances Robertson. UCT Medical Imaging Research Unit, Division of Biomedical Engineering, Department of Human Biology, University of Cape Town, Cape Town, South Africa. Email: Frances.robertson@uct.ac.za.

Background: Repeated glycoCEST MRI measurements on the same subject should produce similar results under the same environmental and experimental conditions. However, fluctuations in the static B_0 field, which may occur between and within measurements due to heating of the shim iron or subject motion, may alter results and affect reproducibility. Here we investigate the repeatability and reproducibility of glycoCEST measurements and examine the effectiveness of a real-time shim- and motion navigated chemical exchange saturation transfer (CEST) sequence to improve reproducibility.

Methods: In nine subjects, double volumetric navigated (DvNav)-CEST acquisitions in the calf muscle were repeated five times in each of two sessions—the first without correction, and the second with real-time shim- and motion correction applied. In both sessions a dynamically changing field was introduced by running a 5-minute gradient intensive diffusion sequence. We evaluated the effect of the introduced B_0 inhomogeneity on the reproducibility of glycoCEST, where the small chemical shift difference between the hydroxyl and bulk water protons at 3 T makes CEST quantification extremely sensitive to magnetic field inhomogeneities.

Results: With real-time shim- and motion correction, glycoCEST results were relatively consistent with mean coefficient of variation (CoV) 2.7%±1.4% across all subjects, whereas without correction the results were less consistent with CoV 84%±71%.

Conclusions: Our results demonstrate that real-time shim- and motion correction can mitigate effects of B0 field fluctuations and improve reproducibility of glycoCEST data. This is important when conducting longitudinal studies or when using glycoCEST MRI to assess treatment or physiological responses over time.

Keywords: Chemical exchange saturation transfer (CEST); field inhomogeneity; glycoCEST; navigator; reproducibility; shim correction

Introduction

Chemical exchange saturation transfer (CEST) is a relatively new MRI contrast that allows indirect detection of low concentration metabolites through chemical exchange of selectively excited bound protons with free water (1-4).

Since the MR signal of the water pool is attenuated by only a few percent, measurements are, however, highly sensitive to any inhomogeneities and motion.

Field homogeneity can be compromised by several factors including subject motion (5,6), breathing, heating of the iron

plates in the shim trays by eddy currents, and mechanical vibrations (7,8) during measurement. Small variations in the field will alter the chemical shifts of nuclei and as such impact the saturation effect that is being measured by CEST yielding inaccurate results, especially in close proximity to the water signal (9). The effects of field inhomogeneity, which may vary between successive CEST acquisitions and scanning sessions, will be even more significant in studies requiring repeated scanning, such as studies of pre- and post-exercise glycogen depletion and repletion, perfusion studies (10-12), and assessment of glucose metabolism using CEST MRI (glucoCEST) in the brain (13-16).

Repeatability assesses the agreement between repeated measurements made using the same method on the same subject under identical conditions, and over a short period of time during which the measured value is assumed to be constant. Variability in such cases reflects the accuracy of the method alone (17). Reproducibility, on the other hand, assesses agreement between measurements made using the same method on the same subject, but under different conditions (17-19), which may be different observers or measurements being made over a period of time.

Under constant experimental conditions CEST offset measurements for the same subject should be repeatable. To be of practical use, measurements in different sessions should also be reproducible, that is robust to instrument-related or environmental variations besides that of the CEST effect itself. Any differences in the CEST data should therefore reflect only physiological variations.

Recently, we introduced a motion- and shim navigated glycoCEST sequence (20) that was shown to decrease the effects of subject motion and field inhomogeneity. To date, the repeatability and reproducibility of this sequence have not been assessed. This work examines the impact of field inhomogeneity caused by heating of the shim irons on the reproducibility of *in vivo* glycoCEST measurements and evaluates the effectiveness of our real-time shim- and motion corrected sequence to improve repeatability and reproducibility.

Methods

Data acquisition

All scans were performed on a Skyra 3 T MRI scanner (Siemens, Erlangen, Germany) using a 15-channel Tx/Rx knee coil according to protocols that had been approved by the Human Research Ethics Committee of the Faculty

of Health Sciences, University of Cape Town. Written informed consent was obtained from all volunteers.

Nine healthy subjects (7 male and 2 females; age: 23–38) were recruited for the study. A high-resolution structural image was acquired for positioning of the CEST slice. Single slice axial CEST images were acquired from the calf muscle of each subject 5 times in each of two sessions; in the first session no shim- or motion correction were applied, and in the second both real-time shim- and motion correction were applied, to allow comparison of the reproducibility of CEST measurements in each case. A typical diffusion tensor imaging (DTI) sequence used in brain research (1 mm isotropic resolution, b value 1,000 s/mm^2) with a duration of five minutes was run between the third and fourth CEST acquisitions for the first 7 subjects, and before the five CEST acquisitions for the remaining 2 subjects. Since heating of the shim irons by the gradient-intensive diffusion scan results in a dynamically changing field during subsequent scans, this allowed us to evaluate the effect of this changing shim on the reproducibility of the CEST data. The DTI sequence can cause field changes of up to 30 Hz due to heating (21), as well as mechanical vibrations (21-24).

Scanning protocols

A 2D gradient echo single-shot echo planar imaging (ss-EPI) continuous wave (CW) CEST sequence with double volumetric navigators (DvNav-CEST) was used for this study. The pair of navigators acquired with different echo times (TEs) allow both shim- and motion to be corrected (20) in real time. The k-space slices of the two navigators are acquired in an interleaved fashion.

The magnitude and phase images of the navigator pairs are generated immediately after acquisition. For pose estimation, the magnitude image of the first 3D navigator in the pair is compared to a reference, selected to be the first navigator after the dummy scans. Prospective acquisition correction (PACE) (25), performed immediately after the navigator acquisition, computes translation and rotation parameters relative to the reference.

Shim correction involves computing a 3D field map by complex division of the images of the DvNav pair. Since DvNav-CEST comprises two interleaved sequences with different field of views (FOVs), two frequency (ΔFs) and first order shim (linear shim gradients G_x, G_y and G_z) estimates are calculated—one for the selected CEST FOV and one for the DvNav FOV. The shim estimate for the DvNav is calculated using an unweighted least squares
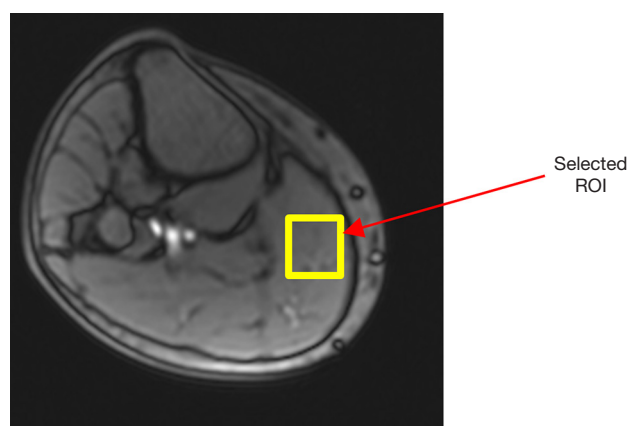
Figure 1 Location of selected ROI used for analysis of glycoCEST data. ROI, region of interest; CEST, chemical exchange saturation transfer.

regression (26).

If motion correction is selected in the protocol, motion estimates are transmitted to the sequence. Slice position and orientation are then updated prior to the next CEST and DvNav measurement. If shim correction is enabled, this is followed by adjustment of the linear shim gradients for both sequences. Frequency correction involves recalculating the frequency and the phase of the radio frequency (RF) and analog-to-digital converter (ADC) pulses for both the DvNav and CEST sequences.

CEST imaging parameters were: repetition time (TR) =2,500 ms, TE =21 ms, FOV =220×220 mm^2, pixel size =3.5×3.5 mm^2, slice thickness =5 mm, 43 offset measurements (including 2 unsaturated reference measurements) acquired with an optimized RF power of 1.5 μT and saturation pulse duration 1,000 ms, swept between –3 and 3 ppm (with respect to water) in intervals of 0.15 ppm. CW RF irradiation parameters had been optimized previously for detection of glycogen in simulations with Bloch-McConnell equations, and subsequently verified *in vitro* for different glycogen concentrations and *in vivo* in human calf muscle (27).

The DvNav parameters were: TR =13 ms, TE$_1$ =4.8 ms and TE$_2$ =7.0 ms, acquisition matrix 32×32×32, 8 mm isotropic voxels (with 6/8 partial Fourier encoding in the slice direction), FOV 256 mm, turbo factor 32, 2° flip angle and bandwidth 4,882 Hz/px. A 2.2 ms echo time difference (ΔTE) was chosen to maintain fat and water in phase. The total data acquisition time, including the navigators, was 1 min and 30 seconds. The navigators were included in the relaxation

time of the CEST sequence. Volunteers were instructed to maintain their position during the whole scanning session.

Data analysis

On the high-resolution structural scan, a 35×35×5 mm^3 region of interest (ROI) was manually selected from the largest muscle group (gastrocnemius) in the calf (*Figure 1*) for glycoCEST analysis. Consistent placement between subjects was achieved by visual comparison. Since there was assumed to be minimal displacement between repeated acquisitions of one subject within a session, the identical ROI position was used. A custom-written Matlab (MathWorks, Inc. 2014) program was used to process all the images and generate CEST spectra and magnetization transfer ratio asymmetry (MTR$_{asym}$) curves. The average of two reference measurements (images without saturation), which were acquired at the beginning of the measurement, was used for normalization when generating the Z-spectra. CEST spectra were generated by fitting a 30th order polynomial to the measured data. An example of the fitted curves along with the raw data is shown in *Figure 2*. In subsequent figures only fitted data are shown. The MTR$_{asym}$ curve was generated by subtracting the intensity of CEST spectra down-field of water (positive offset frequencies) from that up-field of water (negative offset frequencies). For all acquisitions, the MTR$_{asym}$ integral was calculated between 0.5–1.5 ppm downfield of water, targeting glycogen.

To compare retrospective shim correction to the navigator based real-time shim correction, we applied a polynomial fitting field inhomogeneity correction method (28,29) to the CEST spectra acquired from the 8th subject during the uncorrected session. CEST spectra were fitted to a 12th order polynomial, and the frequencies corresponding to the lowest signal intensity in the fitted spectra were assumed to be the water resonance frequency. All spectra were shifted accordingly to correct field inhomogeneity shift effects.

For each participant and session, the standard deviation (Std) and coefficient of variation (CoV) of the MTR$_{asym}$ integrals were calculated to compare reproducibility between sessions with and without shim correction. CoV for each subject i and session j was calculated as follows:

$$CoV_{i,j}\,(\%) = \frac{\sigma_{i,j}}{\mu_{i,j}} \times 100\% \qquad [1]$$

where σ and μ are the Std and means, respectively, of the 5 acquisitions performed in each subject in each session. To investigate measurement repeatability (i.e., measurements
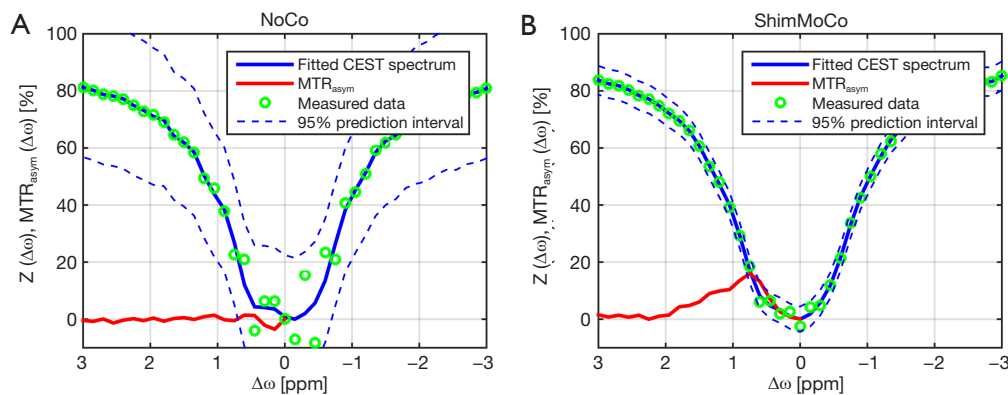
Figure 2 Example dataset showing raw data and 30th order polynomial fits for acquisitions without (A) and with (B) motion and shim correction in a single volunteer. 95% prediction intervals are also shown. CEST, chemical exchange saturation transfer; MTR_{asym}, magnetization transfer ratio asymmetry.

under the same conditions), the CoV and Std were also calculated using only the first 3 pre-DTI acquisitions for the 7 subjects in whom DTI was performed after the 3rd CEST acquisition. For these same 7 subjects, agreement of MTR_{asym} integrals averaged across the first 3 pre-DTI CEST acquisitions from sessions with and without real-time shim- and motion correction was evaluated using Pearson correlation and a Bland-Altman plot.

Results

A total of 90 CEST spectra and MTR_{asym} curves (9 subjects × 5 scans × 2 sessions) were generated and analyzed. *Figure 3* shows the CEST and MTR_{asym} curves for the first 3 subjects from sessions without (NoCo) and with (ShimMoCo) real-time shim- and motion correction. MTR_{asym} curves from CEST acquisitions with real-time shim- and motion correction demonstrate greater consistency between acquisitions compared to those from acquisitions without. Specifically, significant drift is evident in the uncorrected session in the 4th and 5th acquisitions following the DTI acquisition.

Figure 4 shows for both sessions the zero- and first-order shim parameters measured in a single subject during the acquisitions preceding (3rd CEST acquisition) and following (4th CEST acquisition) the DTI acquisition. Drift in the scanner frequency is evident in scan 4 following the gradient intensive DTI sequence for the acquisition performed without correction (NoCo).

For the last two subjects (subjects 8 and 9) the 5-minute DTI acquisition was performed prior to the CEST

acquisitions in both sessions. The CEST spectra and MTR_{asym} curves from both sessions are shown in *Figure 5A,B* for subject 8. Notably, DTI-induced field inhomogeneity in the session without shim- or motion correction (NoCo) results in a flatter CEST spectrum with broadening around 0 ppm and spectral shifts. This causes distortion of the MTR_{asym} curve, which is particularly severe in the first acquisition after DTI. In contrast, CEST acquisitions from the session with real-time shim- and motion correction yield consistent spectra (*Figure 5B*). *Figure 5C* shows the CEST spectra from the session without correction after performing polynomial fitting field inhomogeneity correction. Notably, retrospective field correction failed to recover the MTR_{asym} curve.

Figure 6A shows how the MTR_{asym} integral values of the first 7 subjects vary across the five consecutive scans. Values from acquisitions with real-time shim- and motion correction (solid lines) are higher (mean ± Std: with correction 73%±11%; without shim- or motion correction 27%±14%, P<0.001) and demonstrate greater consistency, even following the DTI acquisition performed before the 4th measurement, than those performed without (dashed lines). A significant reduction in MTR_{asym} integral values is clearly evident following the DTI acquisition in acquisitions performed without shim- and motion correction (mean ± Std: first three acquisitions 34%±13%; last two acquisitions 17%±16%, P=0.042), while values before and after DTI did not differ in acquisitions with real-time shim- and motion correction (mean ± Std: first three acquisitions 72%±11%; last two acquisitions 74%±11%, P=0.77). *Figure 6B* shows the MTR_{asym} integral values for the two subjects whose

1678

Simegn et al. Motion- and shim corrected 2D glycoCEST MRI
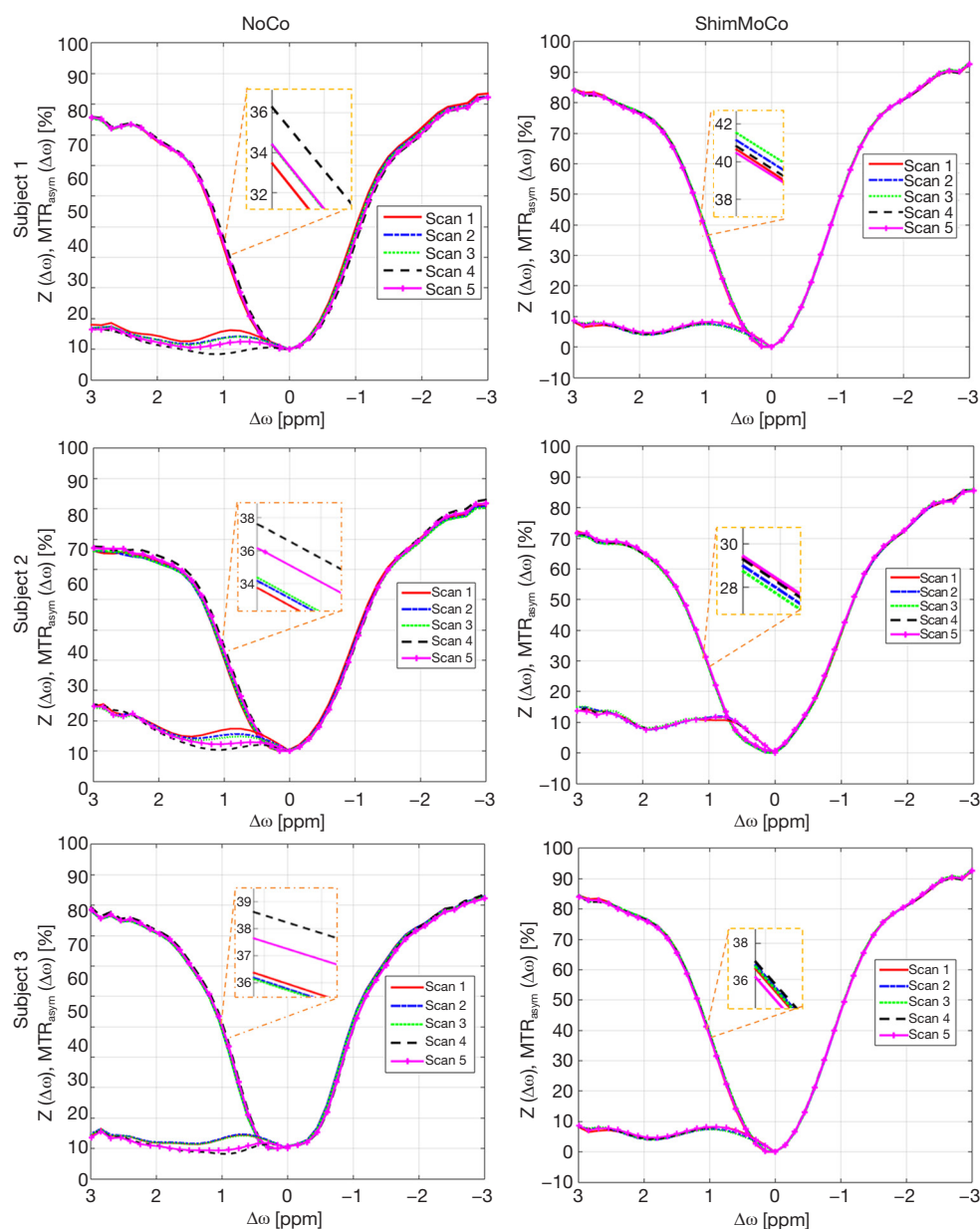
Figure 3 ROI CEST spectra and MTR$_{asym}$ curves in three subjects (1, 2 and 3) for five repeated CEST acquisitions (scans 1 to 5) from sessions without (NoCo; left) and with (ShimMoCo; right) real-time shim- and motion correction, respectively. In both sessions the DTI sequence was run in between the third and fourth CEST acquisition. ROI, region of interest; CEST, chemical exchange saturation transfer; MTR$_{asym}$, magnetization transfer ratio asymmetry; DTI, diffusion tensor imaging.

CEST acquisitions were performed after an initial DTI acquisition. Drift in the MTR$_{asym}$ integral values are evident in the acquisitions performed without shim- and motion correction (dashed lines) due to the fact that the shim is dynamically changing as the shim irons cool.

Table 1 shows for each participant the CoV and Std of the MTR$_{asym}$ integrals from the 5 uncorrected and corrected CEST acquisitions. *Table 2* shows the same, but only for the 3 acquisitions preceding the DTI acquisition (i.e., without deliberate introduction of B$_0$ changes) in the first 7 subjects. *Table 3* shows the reproducibility of the MTR$_{asym}$ integral for a single subject (subject 8) without correction, with real-
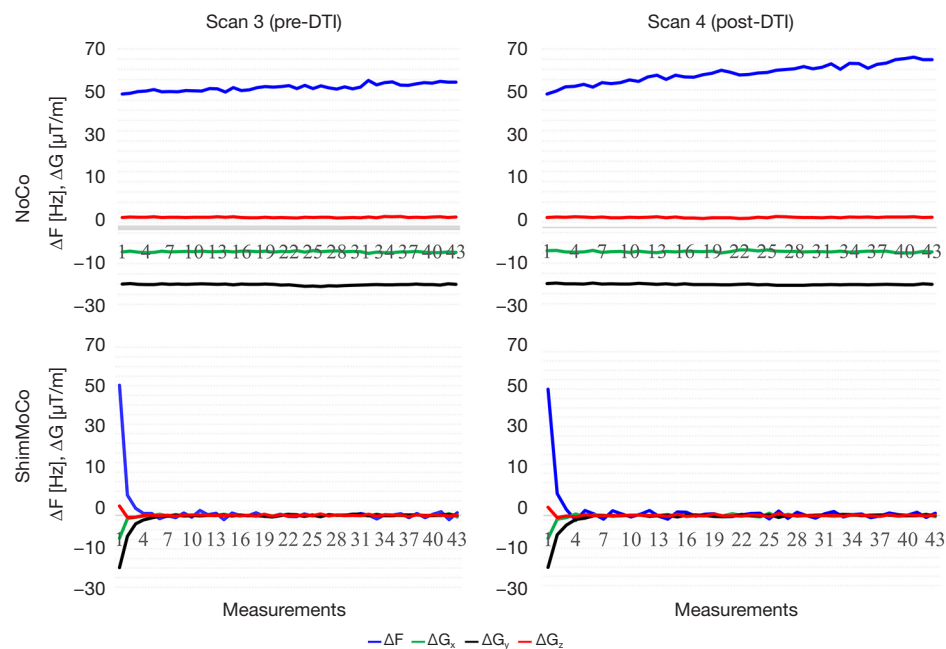
Figure 4 Shim parameters in a single subject for the acquisitions immediately (left) preceding (scan 3) and (right) following (scan 4) the 5-minute DTI acquisition from the sessions without (top row; NoCo) and with (bottom row; ShimMoCo) real-time shim- and motion correction, respectively. In the NoCo session, a frequency drift of approximately 10 Hz/min is observed in the acquisition immediately after the DTI (scan 4). DTI, diffusion tensor imaging.

time shim- and motion correction and with shim correction by postprocessing using a polynomial fitting method. Overall, acquisitions with real-time shim- and motion correction applied show large significant reductions in the CoVs and Stds (all P's <0.005) compared to uncorrected acquisitions, while the CoV and Std of the MTR$_{asym}$ integrals obtained after polynomial fitting is similar to that obtained without correction.

Figure 7A shows the association in the first 7 subjects between mean MTR$_{asym}$ integrals (averaged across the first three pre-DTI CEST acquisitions) from acquisitions with (ShimMoCo) and without (NoCo) real-time shim- and motion correction. Although there is a moderate (albeit not significant) relationship (r=0.62, P=0.1), MTR$_{asym}$ integral values from uncorrected acquisitions are consistently lower. This is clearly evident in the Bland-Altman plot shown in *Figure 7B*.

Discussion

The current work shows that glycoCEST spectra and MTR$_{asym}$ curves acquired with prospective shim- and motion correction were more reproducible and less susceptible

to distortions from saturation asymmetry between corresponding offset measurements caused by changes in B$_0$.

In all 7 subjects in whom DTI was performed after the 3rd glycoCEST acquisition, the MTR$_{asym}$ integral of uncorrected acquisitions was reduced in the 4th CEST acquisition, which was performed directly post-DTI, showing evidence of recovery (about 10%) towards its pre-DTI value on the 5th acquisition (*Figure 3*). The CoV also increased by about 39% for post-DTI acquisitions compared to the pre-DTI acquisitions, highlighting the effect of shim distortion and a dynamically changing shim on glycoCEST reproducibility.

By contrast, glycoCEST spectra and MTR$_{asym}$ curves of successive shim- and motion corrected acquisitions were qualitatively similar, including post-DTI acquisitions, with consistent MTR$_{asym}$ values. With correction, the mean (± Std) MTR$_{asym}$ integral CoV across 7 subjects was 2.7%±1.4% compared to 84%±71% without correction. A CoV of 2.7 % for glycoCEST is comparable to gluCEST reproducibility reported previously in studies involving repeated measurements in five mice (30) and *in vivo* in the human brain at 7 T (31). These studies did not use real-time shim and motion correction.
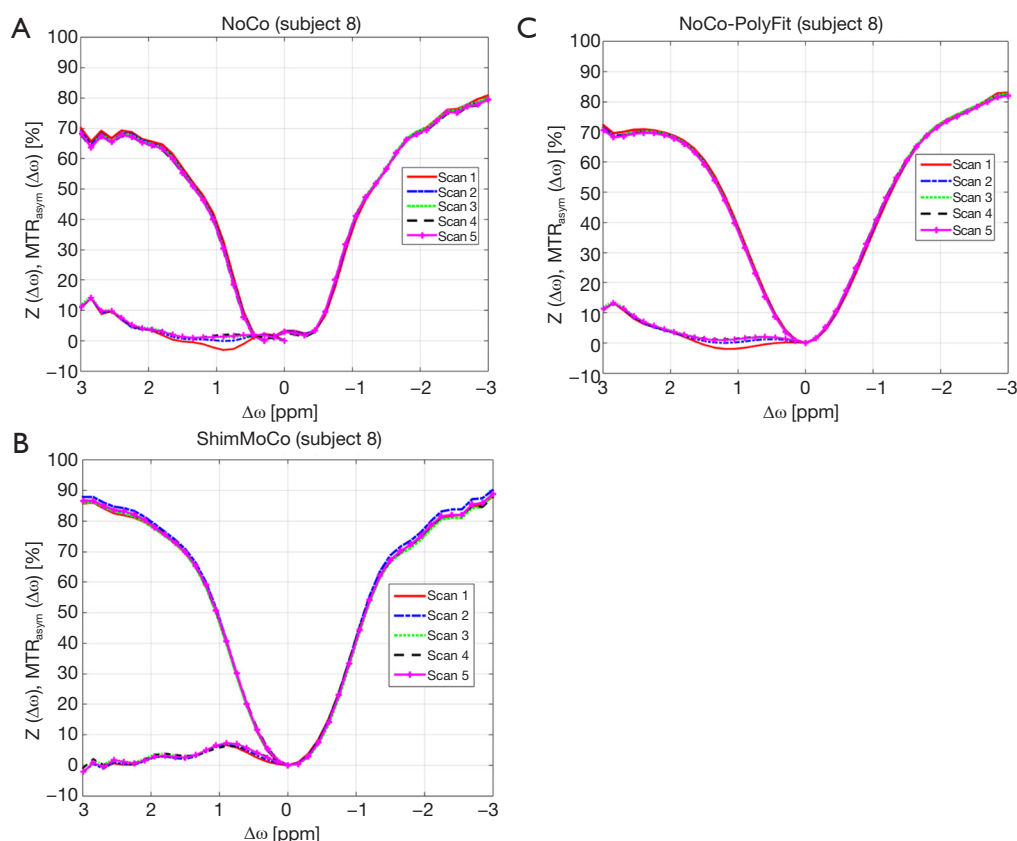
Figure 5 ROI CEST Spectra and MTR$_{asym}$ curves in a single subject (subject 8) for the 5 repeated CEST acquisitions from (A) the session without (NoCo) and (B) the session with (ShimMoCo) real-time shim- and motion correction, respectively. In each session, the five acquisitions were preceded by a 5-minute DTI acquisition; (C) shows curves from the session without any correction after spectral shift correction using a 12th-order polynomial fitting technique (PolyFit). The polynomial fitting technique failed to recover the reduction in the MTR$_{asym}$ integral due to shim distortion. ROI, region of interest; CEST, chemical exchange saturation transfer; MTR$_{asym}$, magnetization transfer ratio asymmetry; DTI, diffusion tensor imaging.
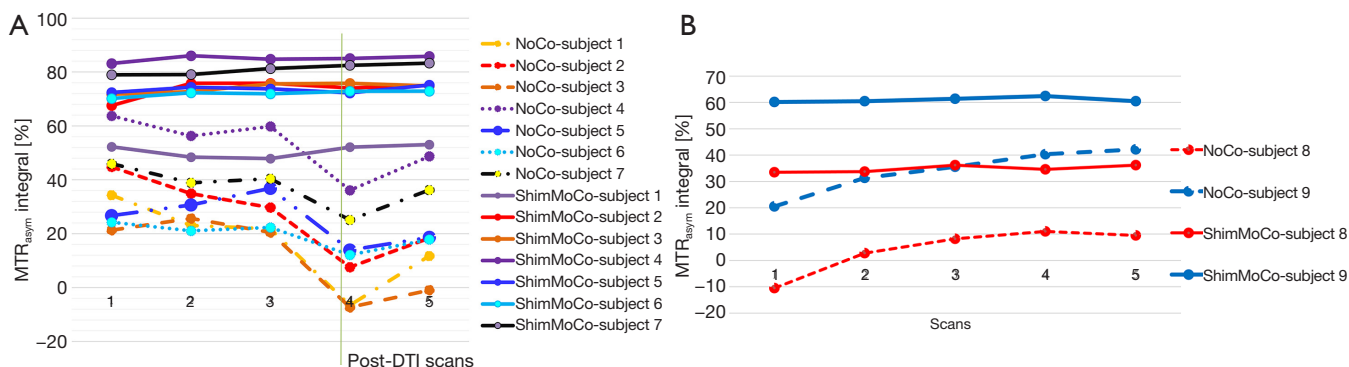
Figure 6 ROI MTR$_{asym}$ integral values in (A) the first 7 and (B) the last 2 subjects for the 5 repeated CEST acquisitions from sessions without (NoCo; dashed lines) and with (ShimMoCo; solid lines) real-time shim- and motion correction, respectively. In the first 7 subjects, the DTI acquisition was performed between the 3rd and 4th CEST acquisition in each session. In the last two subjects, DTI was performed before the first CEST acquisition in each session. ROI, region of interest; CEST, chemical exchange saturation transfer; MTR$_{asym}$, magnetization transfer ratio asymmetry; DTI, diffusion tensor imaging.

Table 1 Comparison of the reproducibility (i.e., under changing conditions), in each of 9 subjects, of the MTR_{asym} integral values from five successive CEST acquisitions performed without (NoCo) and with real-time shim- and motion correction (ShimMoCo), respectively

Volunteers	CoV (%)		Std	
	NoCo	ShimMoCo	NoCo	ShimMoCo
1	91	4.7	15.3	2.4
2	53	4.7	14.5	3.5
3	126	2.4	14.9	1.8
4	21	1.3	10.9	1.1
5	36	1.7	9.2	1.3
6	24	1.5	4.7	1.1
7	21	2.4	7.7	2.0
8	209	3.7	8.8	1.3
9	173	1.5	8.6	0.9

MTR_{asym}, magnetization transfer ratio asymmetry; CEST, chemical exchange saturation transfer; CoV, coefficient of variation; Std, standard deviation.

Table 2 Comparison in the first 7 subjects of the repeatability (i.e., under the same conditions) of MTR_{asym} integral values from the first 3 pre-DTI acquisitions performed without and with real-time shim- and motion correction, respectively

Volunteers	CoV (%)		Std	
	NoCo	ShimMoCo	NoCo	ShimMoCo
1	26	4.8	6.9	2.4
2	21	6.5	7.7	4.8
3	12	2.7	2.8	2.0
4	6	1.7	3.7	1.4
5	16	1.4	5.1	1.0
6	7	1.6	1.6	1.1
7	9	1.6	3.7	1.3

MTR_{asym}, magnetization transfer ratio asymmetry; DTI, diffusion tensor imaging; CEST, chemical exchange saturation transfer; CoV, coefficient of variation; Std, standard deviation.

Zero-order shim (i.e., frequency) changes cause a shift in the entire glycoCEST spectrum leading to a mismatch between the assumed and actual 0 ppm position (32). Without proper shift correction, this causes an increase or decrease in the calculated MTR_{asym} integral depending on the direction of the shift. During all uncorrected acquisitions, a shift (from zero) in zero-order shim

Table 3 Comparison in a single subject (subject 8) of MTR_{asym} integral reproducibility (i.e., under changing conditions) from 5 CEST acquisitions performed after an initial DTI acquisition in the session without any correction (NoCo), the session with prospective shim- and motion correction (ShimMoCo) applied, and retrospective correction by a 12th order polynomial fitting technique (PolyFit) of the uncorrected data

| Correction mechanism	CoV (%)	Std
NoCo	209	8.8
ShimMoCo	4	1.3
PolyFit	173	8.3

MTR_{asym}, magnetization transfer ratio asymmetry; CEST, chemical exchange saturation transfer; CoV, coefficient of variation; Std, standard deviation.

(frequency) was observed. Directly after DTI, the zero-order shim exhibits drift of as much as 10 Hz/min. The presence of field inhomogeneity along slice, phase encoding and readout directions (gradients) can cause a temporal shift, geometric distortion (shearing, stretching, compression, scaling) (33,34), or phase dispersion across affected voxels (5,35,36) resulting in signal loss and positional mis-registration of the signal and the acquired offset images during voxel-wise CEST data analysis.

Although post processing using high-order polynomial fitting (28,29) helps to center the glycoCEST spectrum at the minimum to compensate for shifts of the entire Z-spectrum arising from zero-order shim changes, the technique cannot correct a dynamically changing B_0 that varies between different frequency offset measurements. Although post-processing using 12th order polynomial fitting of the five CEST acquisitions performed after an initial DTI acquisition, reduced the CoV of the MTR_{asym} integrals slightly from the uncorrected case (from 209% to 173%), the variation is still large. This shows that attenuation of the glycoCEST signal due to the cumulative effect of zero-order and first-order shim changes in the presence of a fluctuating B_0 field cannot be corrected using simple post-processing techniques alone, highlighting the need for prospective correction.

Even without the deliberate introduction of B_0 instability, the CoVs for the pre-DTI glycoCEST acquisitions (scans 1–3) were lower for the shim- and motion corrected sessions (mean CoV ± Std =2.9%±2.0%) than for the sessions without correction (mean CoV ± Std =14.0%±7.5%), showing improved measurement repeatability under conditions assumed to be constant. The mean MTR_{asym}

1682

Simegn et al. Motion- and shim corrected 2D glycoCEST MRI
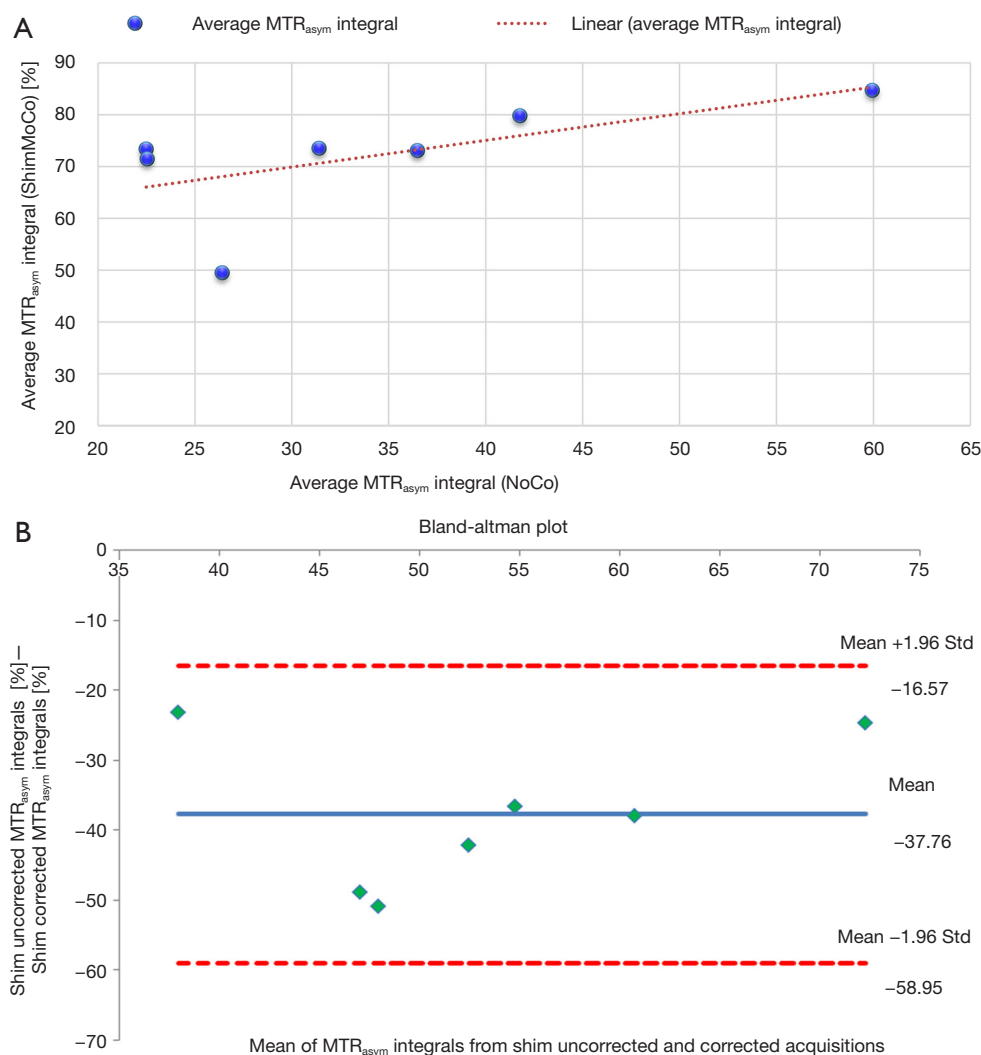
Figure 7 Comparison for the first 7 subjects of MTR_{asym} integrals averaged across the three pre-DTI CEST acquisitions from the session with real-time shim- and motion correction (ShimMoCo) to the equivalent values from the session without any correction (NoCo). The scatter plot in (A) shows the association between values obtained in the two sessions, and (B) the Bland-Altman plot. CEST, chemical exchange saturation transfer; MTR_{asym}, magnetization transfer ratio asymmetry; DTI, diffusion tensor imaging; Std, standard deviation.

integral values were also lower for scans acquired without correction compared to scans acquired with shim- and motion correction applied, suggesting that glycoCEST measurements may be underestimated if a proper shim is not maintained throughout the acquisition.

Considering the mean MTR_{asym} in the pre-DTI acquisitions only (*Figure 7*), the inter-session correlation between ShimMoCo and NoCo measurements was moderate, indicating that similar conclusions about relative glycogen concentrations in subjects could be drawn using an uncorrected or corrected glycoCEST sequence. Although

no gold standard glycogen measurement is available to us to confirm this, we expect the shim- and motion corrected sequence to produce more accurate measurements by correcting for small subject motions and changes in field homogeneity. In addition to producing more repeatable and reproducible within-subject measurements, the shim- and motion corrected acquisitions also demonstrated a lower between-subject CoV (15.3%) for MTR_{asym} than the uncorrected acquisitions (38.7%).

Studies using glycoCEST MRI typically employ multiple scanning sessions to examine changes in physiology,

biochemistry (37), molecular composition (38), metabolism (e.g., muscle glycogen depletion and repletion), and perfusion (39,40). Due to instrumental and physiological factors that influence the CEST effect, longitudinal and multicenter reproducibility is challenging in practice. In addition, the glycoCEST effect may be confounded by other CEST contrasts that appear in the Z-spectrum. Notably we observe reproducible dips at 2.5 and –2 ppm, possibly corresponding to amine protons and the nuclear Overhauser effect (NOE), respectively, that may affect glycogen MTR_{asym} estimation. Technological improvements that address some of these issues will improve the practical utility of glycoCEST imaging.

A handful of studies have examined reproducibility of CEST measurements *in vivo* including amine proton transfer imaging (APTCEST) of the human breast at 7 T (41), glutamate in mice using gluCEST (30) and gray and white matter glutamate contrast in the human brain (31). However, the effect of field inhomogeneity on repeatability and reproducibility of CEST data has not previously been evaluated and to our knowledge no previous study has evaluated the reproducibility of glycogen measurements using CEST MRI.

Our results demonstrate that drift in the scanner center frequency and gradients resulting from shim iron heating affect glycoCEST spectra, leading to inaccurate quantification, and that these effects can be reduced or eliminated with application of prospective shim- and motion correction. This study highlights the importance of correcting field inhomogeneity prospectively during glycoCEST longitudinal studies. The navigated glycoCEST MRI sequence provides highly reproducible measurements in human calf muscle for a comparatively large ROI. Additional work needs to be done to establish the reproducibility of glycoCEST within and across specific regions of the calf muscle.

We acknowledge several other limitations of the current study, including a limited number of subjects. Effects of scanner field strength, RF coil type and environmental factors such as temperature were not assessed; however, we anticipate that this assessment of reproducibility lays the groundwork for further CEST reproducibility studies that will systematically investigate these important questions.

Conclusions

DvNav-glycoCEST acquisitions in the calf muscles of nine subjects, 5 times in each of two sessions, show that

prospective shim- and motion correction produces more repeatable results than uncorrected acquisitions. The effect of B_0 field fluctuations on glycoCEST reproducibility was also demonstrated. Our simultaneous real-time shim- and motion navigated glycoCEST sequence shows the potential to produce reproducible results by mitigating the effect of changes in field homogeneity. The navigated glycoCEST sequence may prove particularly valuable for applications that require multiple scanning sessions, for example to study glycogen depletion and repletion in skeletal muscle.

Footnote

Conflicts of Interest: The authors have no conflicts of interest to declare.

Ethical Statement: All scans were performed on a Skyra 3 T MRI scanner (Siemens, Erlangen, Germany) using a 15-channel Tx/Rx knee coil according to protocols that had been approved by the Human Research Ethics Committee of the Faculty of Health Sciences, University of Cape Town (HREC REF:337/2018). Written informed consent was obtained from all volunteers.

References

1. Zhou J, Wilson DA, Sun PZ, et al. Quantitative description of proton exchange processes between water and endogenous and exogenous agents for WEX, CEST, and APT experiments. Magn Reson Med 2004;51:945-52.
2. Sun PZ, van Zijl PC, Zhou J. Optimization of the irradiation power in chemical exchange dependent

1684

Simegn et al. Motion- and shim corrected 2D glycoCEST MRI

saturation transfer experiments. J Magn Reson 2005;175:193-200.

3. van Zijl PC, Yadav NN. Chemical exchange saturation transfer (CEST): what is in a name and what isn't? Magn Reson Med 2011;65:927-48.

4. Zaiss M, Bachert P. Chemical exchange saturation transfer (CEST) and MR Z-spectroscopy in vivo: a review of theoretical approaches and methods. Phys Med Biol 2013;58:R221-69.

5. Ward HA, Riederer SJ, Jack CR Jr. Real-time autoshimming for echo planar timecourse imaging. Magn Reson Med 2002;48:771-80.

6. Pfeuffer J, Van de Moortele PF, Ugurbil K, et al. Correction of physiologically induced global off-resonance effects in dynamic echo-planar and spiral functional imaging. Magn Reson Med 2002;47:344-53.

7. Foerster BU, Tomasi D, Caparelli EC. Magnetic field shift due to mechanical vibration in functional magnetic resonance imaging. Magn Reson Med 2005;54:1261-7.

8. Benner T, van der Kouwe AJ, Kirsch JE, et al. Real-time RF pulse adjustment for B0 drift correction. Magn Reson Med 2006;56:204-9.

9. Liu G, Gilad AA, Bulte JW, et al. High-throughput screening of chemical exchange saturation transfer MR contrast agents. Contrast Media Mol Imaging 2010;5:162-70.

10. Pekar J, Jezzard P, Roberts DA, et al. Perfusion imaging with compensation for asymmetric magnetization transfer effects. Magn Reson Med 1996;35:70-9.

11. Yeung HN, Aisen AM. Magnetization transfer contrast with periodic pulsed saturation. Radiology 1992;183:209-14.

12. van Zijl PC, Jones CK, Ren J, et al. MRI detection of glycogen in vivo by using chemical exchange saturation transfer imaging (glycoCEST). Proc Natl Acad Sci U S A 2007;104:4359-64.

13. Nasrallah FA, Pagès G, Kuchel PW, et al. Imaging brain deoxyglucose uptake and metabolism by glucoCEST MRI. J Cereb Blood Flow Metab 2013;33:1270-8.

14. Jin T, Mehrens H, Hendrich KS, et al. Mapping brain glucose uptake with chemical exchange-sensitive spin-lock magnetic resonance imaging. J Cereb Blood Flow Metab 2014;34:1402-10.

15. Chan KW, McMahon MT, Kato Y, et al. Natural D-glucose as a biodegradable MRI contrast agent for detecting cancer. Magn Reson Med 2012;68:1764-73.

16. Walker-Samuel S, Ramasawmy R, Torrealdea F, et al. In vivo imaging of glucose uptake and metabolism in tumors. Nat Med 2013;19:1067-72.

17. Bartlett JW, Frost C. Reliability, repeatability and reproducibility: analysis of measurement errors in continuous variables. Ultrasound Obstet Gynecol 2008;31:466-75.

18. Casadevall A, Fang FC. Reproducible science. Infect Immun 2010;78:4972-5.

19. Crook SM, Davison AP, Plesser HE. Learning from the past: approaches for reproducibility in computational neuroscience. In: Bower JM. editor. 20 years of computational neuroscience. New York: Springer, 2013:73-102.

20. Simegn GL, Van der Kouwe AJW, Robertson FC, et al. Real-time simultaneous shim and motion measurement and correction in glycoCEST MRI using double volumetric navigators (DvNavs). Magn Reson Med 2019;81:2600-13.

21. Alhamud A, Taylor PA, van der Kouwe AJ, et al. Real-time measurement and correction of both B0 changes and subject motion in diffusion tensor imaging using a double volumetric navigated (DvNav) sequence. Neuroimage 2016;126:60-71.

22. Truong TK, Chen B, Song AW. Integrated SENSE DTI with correction of susceptibility- and eddy current-induced geometric distortions. Neuroimage 2008;40:53-8.

23. Avram AV, Guidon A, Truong TK, et al. Dynamic and inherent B0 correction for DTI using stimulated echo spiral imaging. Magn Reson Med 2014;71:1044-53.

24. Bodammer N, Kaufmann J, Kanowski M, et al. Eddy current correction in diffusion-weighted imaging using pairs of images acquired with opposite diffusion gradient polarity. Magn Reson Med 2004;51:188-93.

25. Thesen S, Heid O, Mueller E, et al. Prospective acquisition correction for head motion with image-based tracking for real-time fMRI. Magn Reson Med 2000;44:457-65.

26. Hess AT, Tisdall MD, Andronesi OC, et al. Real-time motion and B0 corrected single voxel spectroscopy using volumetric navigators. Magn Reson Med 2011;66:314-23.

27. Simegn GL. Double volumetric navigators for real-time simultaneous shim and motion measurement and correction in glycogen chemical exchange saturation transfer (glycoCEST) MRI. Cape Town: University of Cape Town, 2019. Available online: https://open.uct.ac.za/handle/11427/30039

28. Zhou J, Lal B, Wilson DA, et al. Amide proton transfer (APT) contrast for imaging of brain tumors. Magn Reson Med 2003;50:1120-6.

29. Zhou J, Blakeley JO, Hua J, et al. Practical data acquisition method for human brain tumor amide proton transfer (APT) imaging. Magn Reson Med 2008;60:842-9.

30. Bagga P, Pickup S, Crescenzi R, et al. In vivo gluCEST MRI: reproducibility, background contribution and source of glutamate changes in the MPTP model of Parkinson's disease. Sci Rep 2018;8:2883.

31. Nanga RPR, DeBrosse C, Kumar D, et al. Reproducibility of 2D gluCEST in healthy human volunteers at 7 T. Magn Reson Med 2018;80:2033-9.

32. Wu B, Warnock G, Zaiss M, et al. An overview of CEST MRI for non-MR physicists. EJNMMI Phys 2016;3:19.

33. Mark Haacke E, Thompson MR, Venkatesan R, et al. Magnetic resonance imaging: physical principles and sequence design. New York: Wiley-Liss, 1999.

34. Bammer R, Skare S, Newbould R, et al. Foundations of advanced magnetic resonance imaging. NeuroRx 2005;2:167-96.

35. Reber PJ, Wong EC, Buxton RB, et al. Correction of off resonance-related distortion in echo-planar imaging using EPI-based field maps. Magn Reson Med 1998;39:328-30.

36. Wachowicz K, Tadic T, Fallone BG. Geometric distortion and shimming considerations in a rotating MR-linac design due to the influence of low-level external magnetic fields. Med Phys 2012;39:2659-68.

37. Sun PZ, Sorensen AG. Imaging pH using the chemical exchange saturation transfer (CEST) MRI: correction of concomitant RF irradiation effects to quantify CEST MRI for chemical exchange rate and pH. Magn Reson Med 2008;60:390-7.

38. Haris M, Singh A, Cai K, et al. MICEST: a potential tool for non-invasive detection of molecular changes in Alzheimer's disease. J Neurosci Methods 2013;212:87-93.

39. Haris M, Cai K, Singh A, et al. In vivo mapping of brain myo-inositol. Neuroimage 2011;54:2079-85.

40. Anemone A, Consolino L, Longo DL. MRI-CEST assessment of tumour perfusion using X-ray iodinated agents: comparison with a conventional Gd-based agent. Eur Radiol 2017;27:2170-9.

41. Klomp DW, Dula AN, Arlinghaus LR, et al. Amide proton transfer imaging of the human breast at 7T: development and reproducibility. NMR Biomed 2013;26:1271-7.